Constrained molecular dynamics for quantifying intrinsic ductility versus brittleness

D. Tanguy*

CNRS, UMR 5146, Ecole des Mines de Saint-Etienne, 158 cours Fauriel, Fr-42023 Saint-Etienne, France and Centre Européen de Calcul Atomique et Moléculaire, Ecole Normale Supérieure, 46 Allée d'Italie, Fr-69007 Lyon, France

(Received 1 July 2007; revised manuscript received 27 August 2007; published 30 October 2007; publisher error corrected 12 November 2007)

Evaluating the critical load levels for intrinsic ductility and brittle propagation is a first, but necessary, step for modeling semibrittle crack propagation. In the most general case, the calculations have to be fully atomistic because the details of the crack tip structure cannot be captured by continuum mechanics. In this paper, we present a method to explore ductile and brittle configurations, within the same force field, giving a quantitative estimate of the proximity of a transition from intrinsic ductility to brittleness. The shear localization is characterized by a centrosymmetry criterion evaluated on each atom in the vicinity of the crack tip. This provides an efficient order parameter to track the nucleation and propagation of dislocations. We show that it can be used as a holonomic constraint within molecular dynamics simulations, giving a precise control over plasticity during crack propagation. The equations of motion are derived and applied to crack propagation in the $[11\bar{2}]$ direction of an fcc crystal loaded in mode I along [111]. The critical loads for dislocation emission and for brittle propagation are computed. The key point is that the generalized forces of constraint are not dissipative. Therefore, they do not spoil the critical elastic energy release rates (the Griffith criterion is preserved). As an example of the possibilities of the method, the response of blunted tips is investigated for three configurations: a slab of vacancies, an elliptical hole, and a circular hole. Brittle propagation by an alternative mechanism to cleavage, called "vacancy injection," is reported.

DOI: 10.1103/PhysRevB.76.144115 PACS number(s): 62.20.Mk, 02.70.Ns, 61.72.Bb

I. INTRODUCTION

Some materials, such as bcc iron or silicon, have a critical temperature T_c below which they can break by cleavage, i.e., cracks propagate along crystallographic planes, creating almost atomistically flat surfaces. Above T_c, dislocations become mobile and provide the system with a much cheaper way to release the stored elastic energy: plastic deformation. When the dislocation density becomes too high, the microstructure collapses and voids are created. The solid breaks by void coalescence. Fracture becomes ductile. The limit between these two mechanisms is not sharp.[1] In particular, when the samples are prestrained, it is possible to observe cleavage in the presence of plastic deformation: semibrittle fracture. This mechanism is of particular importance since many structural metallic alloys fail by this mechanism: ferritic steels at the vicinity of T_c,[1] aluminum alloys AlZnMg (Ref. 2) and Ni based alloys[3] when subjected to intergranular hydrogen embrittlement, etc. This problem is multiscale in essence since propagation depends on the details of the crack tip structure (blunted, atomistically sharp, etc.) and of its response (bond breaking or dislocation emission), but the elastic energy to be released is stored in an extended region around the crack.

More specifically, in systems where dislocations easily nucleate and propagate, the plastic zone screens the applied mechanical load. Before explaining the concept of crack tip shielding, let us remind the main result from continuum fracture mechanics. The stress field, in a cracked elastic body, is singular at the crack tip. The singularity is characterized by a single parameter: the stress intensity factor K. K is a scalar which contains the specificity of the system (crack length, sample geometry, mechanical load at the borders). It means that two different systems (let us say a nanometric crack under a huge load and a macroscopic crack under a low load) have exactly the same stress field at the vicinity of the tip, if K is the same in both configurations. When a dislocation nucleates, its stress field produces a singularity at the crack tip of the same shape as the one of the crack alone. It is characterized by its own stress intensity factor k_d. By superposition of linear elastic solutions, the singularity at the crack tip in the presence of a dislocation "cloud" is the sum of the applied K, K_{app}, and the contribution of each individual dislocation: $k=K_{app}+\Sigma_i k_d^i$. When k is lower than K_{app}, the external load is said to be "shielded" by the plastic zone.[4] The modeling of semibrittle fracture should consider the dynamics of the formation of the plastic zone, in competition with "brittle" crack propagation. Nowadays, crack tip plasticity can be modeled, in two dimensions, by discrete dislocation dynamics.[1,4,5] These simulations provide the evolution of the local stress intensity factor k during the formation of the plastic zone. The response of the tip to this effective load is what is left to be quantified at the atomic scale.

Here, following Rice and Thomson,[6] we consider the competition between brittle propagation and emission of a straight dislocation from the crack tip. This is the intrinsic ductility, which is distinguished from the plastic growth of holes and crack blunting by dislocations emitted from remote sources. The simple configuration overestimates the critical load for plastic relaxation since the distribution of sources around and along the tip plays an important role.[7] Nevertheless, it is a necessary condition for cleavage that propagation should happen at a lower load than intrinsic ductility. The Rice and Thomson model, initially based on continuum elasticity results for the dislocation and for the crack, has been refined along the years to take into account the influence of the lattice: first, in the Peierls-Nabarro framework[8] where the unstable stacking energy γ_{us} has been introduced to describe

the energy barrier that the system has to overcome to emit the dislocation, and then, using a mixed atomistic and elastic model based on lattice Green's functions. The goal was to find a criterion able to predict which materials are intrinsically ductile as a function of a limited set of physical parameters: the unstable stacking energy (γ_{us}), the surface energy (γ_s), and the elastic constants (C_{ij}). A set of rules has been proposed and systematically compared with crack tip simulations. The force law is a cohesive zone model whose parameters are modified to explore a range of values for γ_{us}, γ_s, and C_{ij}. The conclusion from this work is that in the homogeneous case,[9,10] it is possible to correlate the intrinsic ductility and/or brittleness of a material with a few physical parameters such as γ_{us} and the energy to create a ledge at the crack tip. However, when an interface is considered,[11] the ledge formation energy will be affected in a complex way by the properties of the interface (the effective force law between the particles of the interface, the coordination, the localization of the emerging dislocation, etc.), which justifies a full atomistic treatment. The purpose of this paper is to present an atomistic method to achieve such calculations.

A practical way of testing the brittleness of a configuration needs to be developed. Here, the term configuration refers to a set of positions and chemical nature of particles and possibly vacancies, in a crystalline bulk, whether perfect or containing defects such as grain boundaries. The usual way of assessing the cohesion of such a structure is by the Griffith criterion. It is a balance between the elastic energy which is restored when the crack grows by an infinitesimal amount and the energy that has to be spent to extend the free surfaces. A convenient formulation is obtained by introducing the elastic energy release rate G ($G=dE/da$, where E is the stored elastic energy and a is the crack length): $G=2\gamma_S$, where γ_S is the surface energy. To finish with the fracture basics, we recall that G and k are related. In the following, we will use both the energetic (G) and stress field (k) characterization of the mechanical load in order to link atomistics with continuum elasticity. Despite the usefulness of the Griffith criterion, several studies at the atomic scale show that a crack does not necessarily follow a path which produces the surfaces of minimum energy. It is particularly striking in Si,[12] where perfect cleavage can be obtained in the $\{110\}$ plane if the crack propagates along $\langle\bar{1}10\rangle$, whereas crack branching is observed if the propagation is forced along $\langle 001\rangle$. This dependence on the propagation direction is not present in the continuum description. *Ab initio* calculations[12] have shown that, in this covalent material, the individual bond breaking events at the crack tip, and the energy barriers associated with them (lattice trapping), are responsible for the crack path. In metals, where the many body character of the bonding is stronger, the effect of the lattice is expected to be smaller in the homogeneous systems. In heterogeneous systems, such as interfaces, or when chemistry is involved, similar effects can be expected. A very nice example is the zigzag path of a crack in NiAl,[13] where high energy, instead of flat, low energy, surfaces are created.

Thus, if the cohesion of a configuration has to be evaluated, a test crack has to be propagated as it can find the path of minimum resistance all by itself. Usually, when a crack is created and loaded in an intrinsically ductile structure, such as fcc, the system has a strong tendency to relax by emitting partial dislocations. It is difficult to explore the brittle configurations at the atomic scale because $k_{\mathrm{I}c}$ (the critical load for brittle propagation in mode I, traction) is high, the crack length is small, and therefore the average stress levels are huge, sometimes approaching the theoretical elastic limit. Partial dislocations, dipoles, or twins can nucleate and considerably shield the crack tip. In this paper, we present a somewhat "radical" approach to semibrittle fracture, in the sense that we believe that realistic shielding has to be treated at a higher length scale. Therefore, we try to decouple plasticity from brittle propagation in our simulations. We show that constrained molecular dynamics can be developed into a powerful tool which gives a precise control over the plasticity in the vicinity of the crack tip. Upon releasing the constraint, the normal intrinsically ductile dynamics is retrieved. The critical k for emission of the first dislocation from the tip $k_{\mathrm{I}e}$ is computed. Switching on the constraint gives access to the brittle configurations and to $k_{\mathrm{I}c}$. The influence of the crack shape is studied (sharp and blunted). Going back to the Rice and Thomson model, the comparison of $k_{\mathrm{I}e}$ with $k_{\mathrm{I}c}$, not only shows if the configuration is ductile but also quantifies the proximity of the transition from intrinsic ductility to brittleness. This would be particularly useful when dealing with the impact of chemical segregation, where the influence of the impurity content on $k_{\mathrm{I}e}$ and $k_{\mathrm{I}c}$ could be followed. For the moment, we focus on the method, tested in a pure metal.

In the reminder of this paper, the constraints are first made explicit, and then, the constrained equations of motion are derived and implemented in molecular dynamics (MD). In the second part, the method is tested in a classical configuration: a flaw in a two dimensional isotropic elastic media submitted to a mode I loading. The critical load for emitting the first partial dislocation and for brittle propagation are evaluated. The link to continuum fracture mechanics is explored. Finally, as an example of the potentialities of the method, blunted crack tips are studied.

II. SIMULATION METHODS

A. Constrained molecular dynamics

We present here a set of equations of motion for molecular dynamics simulations which take into account a constraint in order to create and propagate a brittle crack in an otherwise intrinsically ductile crystal. The general idea is to measure the shear localization and constrain the particles so as to disable the local shear increasing until the unstable stacking configuration is reached and a dislocation is emitted. The shear localization is efficiently measured by a centrosymmetry parameter P,[14] evaluated on each atom:

$$P = \sum_{j=1,6} \|\vec{R}_j + \vec{R}_{j+6}\|^2, \tag{1}$$

where $\vec{R}_j$ and $\vec{R}_{j+6}$ are vectors (or pairs) pointing from the particle toward its first neighbors (12 vectors in the fcc structure). The pairs labeled j and $j+6$ are opposite in the perfect structure and sum to zero. The same pairs are considered

when the crystal is deformed. Sum (1) remains close to zero when the crystal is elastically deformed because the pairs j and $j+6$ remain almost opposite. On the contrary, if a dislocation shears the crystal and if its glide plane cuts a pair, the vectorial sum $\vec{R}_j+\vec{R}_{j+6}$ becomes equal to its Burgers vector $\vec{b}$ and P takes a large value. In the following, we use a slightly different version of this order parameter:

$$\mathrm{CS}_i = \sum_j (\vec{q}_j - \vec{q}_i + \vec{q}_{j+6} - \vec{q}_i) \cdot \vec{b} \leqslant \mathrm{CS}, \tag{2}$$

where i is the index of the particle and the pairs $\vec{R}_j$ are split to explicitly show the position of the particle $\vec{q}_i$ and of its first neighbors $\vec{q}_j$. The vectorial sum over the opposite pairs is now projected on a vector $\vec{b}$ which represents the direction in which the shear localization needs to be controlled. For example, if a Shockley partial glides on a {111} plane of the fcc structure and passes close to i, CS_i jumps from zero to $3\vec{b}^2$, if $\vec{b}$ is the Burgers vector of the partial. The constraint, given by Eq. (2), that has to be verified by a truly brittle crack is that CS_i is always smaller than a critical value [CS in Eq. (2)], physically related to the critical local shear necessary to form the dislocation at the crack tip. CS_i can be thought of as an analogy to the relative displacement ν introduced in Ref. 15.

Constrained molecular dynamics (CMD) is an efficient method for modeling rigid and semirigid molecular systems[16,17] where some bond lengths need to be controlled. It has been extended to different thermodynamic ensembles such as the isothermal-isobaric (NpT).[18,19] CMD is also used to study rare events and compute free energy barriers (for a review, see Ref. 20). In the same spirit and following,[21] we use the principle of Hamilton to derive classical equations of motion which respect the constraint given in Eq. (2). This states that the motion is such that the integral of the Lagrangian over a time interval is stationary with respect to a variation of the path, in configuration space, which connects the configurations at time t_1 and time t_2. The variation (δI) of this integral, for an unconstrained system, is therefore zero:

$$\delta I = \int_{t_1}^{t_2} dt \sum_i \left(\frac{\partial L}{\partial q_i} - \frac{d}{dt}\frac{\partial L}{\partial q_i} \right) \delta q_i = 0, \tag{3}$$

where δq_i represents a variation of the component of the path which corresponds to the position of particle i. The terms in Eq. (3) cannot be set to zero because they are connected through the constraints. Let us consider an N particle system of which n particles are constrained according to Eq. (2). Differentiating Eq. (2) gives n relations connecting the δq_i's (assuming $\mathrm{CS}_i=\mathrm{CS}$, the $\leqslant$ will be considered later). The redundant variables in Eq. (3) can be eliminated using Lagrange multipliers (λ_{i_c}):

$$\int_{t_1}^{t_2} dt \sum_i \left(\frac{\partial L}{\partial q_i} - \frac{d}{dt}\frac{\partial L}{\partial \dot{q}_i} \right) \delta q_i + \sum_{i_c} \lambda_{i_c} \sum_j (\delta q_j + \delta q_{j+6} - 2\delta q_{ic}) \cdot \vec{b} = 0, \tag{4}$$

where the index i represents a particle, i_c represents a constrained particle, and j represents one of the first neighbors of site i. Let us also consider that the $N-n$ first δq_i's are independent variables; therefore, the corresponding terms in Eq. (4) can be set to zero since the integral is zero regardless of the variation δq. This yields $N-n$ equations of motion. The Lagrange multipliers are then chosen so that the n remaining terms in Eq. (4) are zero (n equations). So far, we have obtained N equations of motion, but the n Lagrange multipliers are still undetermined. For a constrained particle k or a neighbor of a constrained particle,

$$\vec{f}_k - m_k \ddot{\vec{q}}_k - z\epsilon\lambda_k \vec{b}_k + \sum_{j_c} \lambda_{j_c} \vec{b}_{j_c} = \vec{0}, \tag{5}$$

where $z=6$ if only the neighbors outside of the glide plane are considered in Eq. (2) or $z=12$ otherwise. Also, $\epsilon=1$ if the particle is constrained or $\epsilon=0$ if the particle is only a neighbor of a constrained particle. Note that the configurational forces are aligned along the Burgers vectors (here, the Burgers vectors have the index of the particle since there is no reason that all particles should be constrained in the same shear direction). For a regular particle k,

$$\vec{f}_k - m_k \ddot{\vec{q}}_k = \vec{0}. \tag{6}$$

The n Lagrange multipliers are finally found by inserting Eqs. (5) and (6) into Eq. (2) after doubly differentiating it with respect to time:

$$\forall i_c \quad \sum_j (\ddot{q}_j + \ddot{q}_{j+6} - 2\ddot{q}_{i_c}) \cdot \vec{b}_{i_c} = 0. \tag{7}$$

As the constraints are not independent, Eq. (7) forms a set of coupled linear equations:

$$A\lambda + B = 0, \tag{8}$$

where λ and B are vectors of dimension n and A is a square matrix whose lines are

$$B_i = \frac{z}{m_i}\vec{f}_i \cdot \vec{b}_i - \sum_j \frac{1}{m_j}\vec{f}_j \cdot \vec{b}_i, \tag{9}$$

$$(A\lambda)_i = z^2 \frac{\lambda_i}{m_i} b_i^2 - \frac{z}{m_i}\sum_{j_c} \lambda_{j_c} \vec{b}_{j_c} \cdot \vec{b}_i - z\sum_{j_c} \frac{\lambda_{j_c}}{m_{j_c}} \vec{b}_{j_c} \cdot \vec{b}_i + \sum_j \sum_{k_c} \frac{\lambda_{k_c}}{m_j} \vec{b}_{k_c} \cdot \vec{b}_i, \tag{10}$$

where j is a neighbor of i, j_c is a constrained first neighbor of i, and k_c is a constrained first neighbor of j. The two first sums are over the constrained first neighbors of site i, whereas the last sum is over the constrained first neighbors of the first neighbors of site i.

The implementation in MD is straightforward: the forces are first computed, and then the CS_i are measured in the area where the constraint is to be applied (i.e., in the example given below, the particles are constrained on the next nearest plane above and below the crack plane). All the n particles which satisfy $CS_i \geqslant CS$ are then put in a list of constrained particles. Equation (8) is built and inverted to get the Lagrange multipliers. Finally, the positions are updated using a Verlet-like algorithm, which includes the generalized forces of constraint $\lambda_i \vec{b}_i$ [Eq. (5)]. As the list is updated at each integration step, the region where the constraints are applied automatically follows the crack tip in the case of propagation. When the Burgers vectors are those of partial dislocations, the constraint forces have a clear physical meaning: they prevent any attempt of the system to reach the unstable stacking configuration, as if the unstable stacking fault was high. Of particular interest is the fact that this result is not obtained by modifying the potential, since the forces originate from the configuration of the first neighbor shell and not from the gradient of the potential. Therefore, the energetics are that of the "real system" and the constraint motion is only used to drive the system through the brittle configurations. In particular, it gives access to the energy of brittle configurations, which can be directly compared to the unconstrained (intrinsically ductile) ones. Ductile to brittle transition can be spotted, in the framework of the Rice and Thomson model.

B. Crack simulation setup

For simplicity, cracks are studied in a two dimensional (2D) geometry which mimics the mathematical problem of a slit of length $2a$ in an infinite isotropic elastic media, in plane strain, submitted to a traction perpendicular to the crack plane (mode I). The simulation box is a thin parallelepiped whose sides are defined by the axes $x=[1\bar{1}0]$, $y=[11\bar{2}]$, and $z=[111]$. A traction is applied in the z direction by means of a constant displacement of the border $\bar{U}$. Periodic boundary conditions are applied along the x and y directions. The system sides are not relaxed ($\epsilon_{xx}=\epsilon_{yy}=0$ on the borders). The crack plane is (x,y). Box sizes used vary between $12\times110\times84$ unit cells (665 280 particles) and $12\times130\times148$ (1 385 280 particles) for crack lengths $2a$ in between 16 and 32 lattice parameters (6 and 12 nm). Therefore, the box size is between five and ten times the crack length in the y direction, this minimizing the interaction with the image (even if it is not zero), and between eight and ten times the crack length in the z direction. The "small" cracks are embedded in a system big enough that the difference between imposed displacements and imposed stresses is small.[22] This does not apply for the bigger cracks anymore but we will see that this is of no importance as long as the load is characterized by a local measure such as the stress intensity factor (k) or the path-independent J integral.

The particles interact via an empirical potential for Al,[23] which reproduces by construction, amongst other properties, the elastic constants and the stacking fault energy. The potential also reproduces quite well the unstable stacking fault energy [0.180 eV/a_0^2, and *ab initio* 0.185 eV/a_0^2 (Ref. 24)], the theoretical strength, the critical displacement,[25] and the displacement where the interaction between two parallel surfaces is negligible [10.4 GPa and *ab initio* 10.9 GPa,[25] $0.14a_0$ and *ab initio* $0.13a_0$,[25] and $1.06a_0$ and *ab initio* $0.87a_0$ (Ref. 26)]. One limitation, which is common for such force fields, is that it underestimates the formation energy of the {111} surface [0.764 J/m^2, *ab initio* 1 J/m^2,[27] and experiment 1.14 J/m^2 (Ref. 28)]. Therefore, the reader should keep in mind that we underestimate the Griffith load ($G=2\gamma_S$) with respect to the experimental value. The above mentioned quantities (elastic constants, theoretical strength, critical displacement) define the main characteristics of the stress-opening relation defining the binding between two {111} planes. It can be obtained by separating, rigidly, the crystal in two blocks.[26] The opening is the extra distance put in between the planes to separate them. A zero opening corresponds to the distance between the planes in a perfect crystal. This relation, sometimes called cohesive zone (CZ) model, could in principle be used as a boundary condition in continuum mechanics in order to describe the stress-opening profile at the crack tip. These data can be extracted directly from the equilibrium crack tip structure obtained by MD more precisely: from the virial stress profile and the opening profile. The equivalence between the CZ and the actual stress-opening relation is not trivial[29] (especially if one wants to include some relaxations in the definition of CZ), but we have checked that in the particular case of an atomistically sharp tip, with the present potential, the two descriptions coincide. As the empirical CZ and the *ab initio* data are in good agreement, as shown above (apart from considerable oscillations in the tail of the stress/displacement curve), the structure of sharp tips obtained with this potential should not be too exotic.

A crack is introduced in the system by "cutting the bonds"[22] which cross the crack area defined by the crack center y_{crack} and its mathematical length $2a_0$. This geometry gives an infinite crack front along the x axis and also an infinite dislocation line when one is emitted. The isotropic elastic solution for a crack in an infinite body is used as a starting configuration before relaxation. The system is relaxed by damped molecular dynamics until the maximum force is at least lower than 10^{-3} eV/Å, but most of the time it is of the order of 10^{-5} eV/Å when the crack is static. The configurations are generated as a function of $\bar{U}$ for different box shapes and crack length $2a$. This 2D geometry (Fig. 1) is representative of three dimensional cracks lying in {111} planes, since small circular cracks relax into hexagons whose segments have precisely the orientation retained for the 2D crack.

III. SHARP CRACKS

We illustrate the efficiency of the centrosymmetry (CS) parameter by studying partial dislocation emission from the crack tip. Using the geometry shown in Fig. 1, the slip system with maximum shear stress is $[112]$ $(11\bar{1})$. When a Shockley partial is emitted from the crack tip, its Burgers

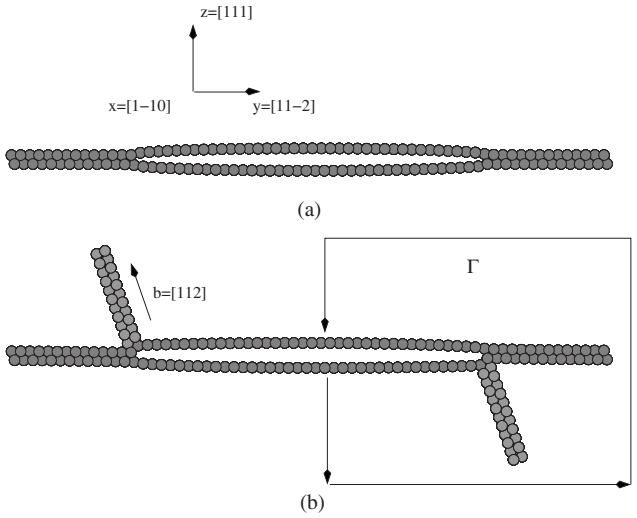

FIG. 1. Unconstrained cracks loaded in mode I (traction) at a level (a) just below the critical stress intensity factor for emission of the first Shockley partial dislocation $k_{I,e}$ and (b) just above $k_{I,e}$. The local plastic shear is measured by a centrosymmetry (CS) order parameter. The light gray particles have a CS parameter higher than $0.1a_0^2$. They belong to the {111} planes above and below the glide plane of the dislocation. Crack blunting is visible on (b). The closed path Γ used to calculate the J integral is represented by arrows in (b).

vector is along [112] and its glide plane is $(11\bar{1})$ (Fig. 1). The Burgers vector $\vec{b}$ in Eq. (2) is set to [112]. CS_i is measured along the next nearest neighbor planes of the crack plane. The profile (Fig. 2) for the upper plane exhibits two discontinuities close to 60 and 76. The first one is related to the formation of a displacement discontinuity which is the signature of the shear localization at the position where the partial dislocation will be emitted. It corresponds to the left partial in Fig. 1(b). The second peak does not lead to a new dislocation when the load is further increased. If one considers the Thompson tetrahedron, there is only one {111} plane which intersects the crack tip (to have two symmetrical {111} planes intersecting the tip, the crack must lie along a P{110} plane with tip along ⟨110⟩). However, the elastic field is symmetric with respect to the crack plane and gives two shear lobes, which leave their signature on the CS profile, but only one of them corresponds to the {111} plane intersecting the tip. The profile along the lower plane is the symmetric of the upper plane profile, with respect to the center of the crack [the symmetry is visible in Figs. 1(b) and 2]. The emission is described in detail in Refs. 15 and 30; when the load increases, the relative displacement between the planes above and below the mathematical glide plane increases at the emergence of the slip plane at the crack tip, until it reaches a critical value where a fully formed dislocation pops out of the crack front. Figure 1 shows the crack morphology just before and just after emission. The light gray particles are those which have a CS parameter higher than 0.1. They span over two $(11\bar{1})$ planes surrounding the glide plane of the partial. In Fig. 3, the maximum CS parameter, extracted from profiles like Fig. 2, is represented as a function of the applied load, characterized by the stress intensity factor. The "S" shaped curve clearly indicates the gradual increase of the shear localization until the unstable configuration is reached. The critical load is approximately $k_{I,e} \approx 0.64 k_{I,G}$, where $k_{I,G}$ is the Griffith stress intensity factor given by $\sqrt{2\gamma_S E' \alpha}$. E' is the Young modulus in plane strain, γ_S is the surface energy, and α is a multiplicative constant given below.

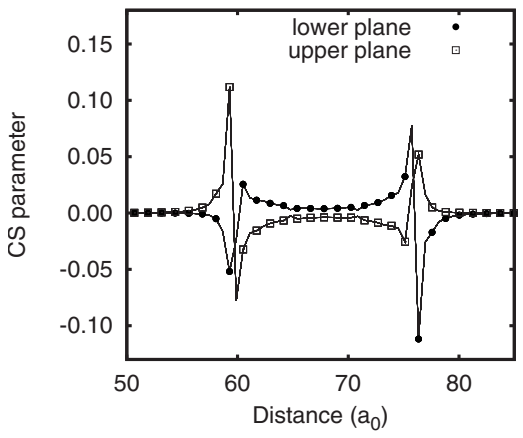

FIG. 2. Centrosymmetry parameter CS_i profile along the crack (measured on the next nearest planes above and below the crack plane). The peaks, with a change of sign, identify the emergence of the shear localization on the crack surface. At higher loads, two peaks emerge and lead to the formation of the partial dislocations seen in Fig. 1. (⊡) upper plane, (●) lower plane.

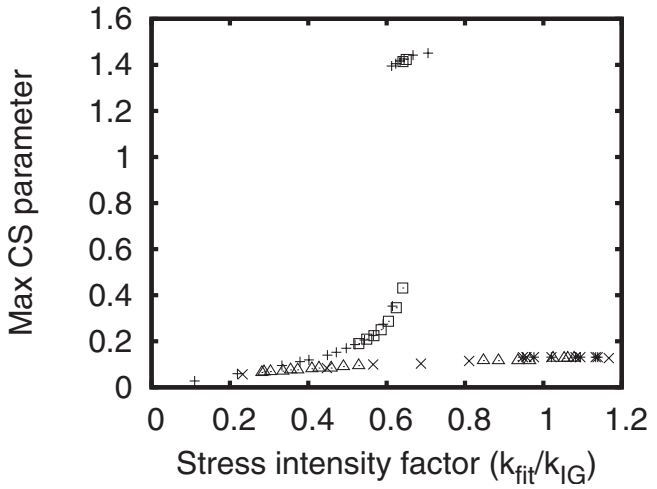

FIG. 3. CS parameter (maximum value in the next nearest neighbor plane from the crack plane) as a function of the stress intensity factor for unconstrained cracks [(+) crack size $2a=16a_0$ in the small system, (⊡) $2a=32a_0$ in the big system] and for a constraint crack [(×) $2a=16a_0$, (△) $2a=16a_0$ with bonds cut, (∗) $2a=32a_0$ with fully restored interactions across the crack], loaded at increasing $\bar{U}$.

The mechanism behind load characterization deserves additional details. In the small size system of Fig. 1, the box size is big enough to compare the stress fields directly with the continuum mechanics solution by Inglis, following Ref. 31. The stress tensor is given by the virial formula, on each atom, without volume correction.[31] Even if the meaning of this definition is controversial, it has been shown that at T

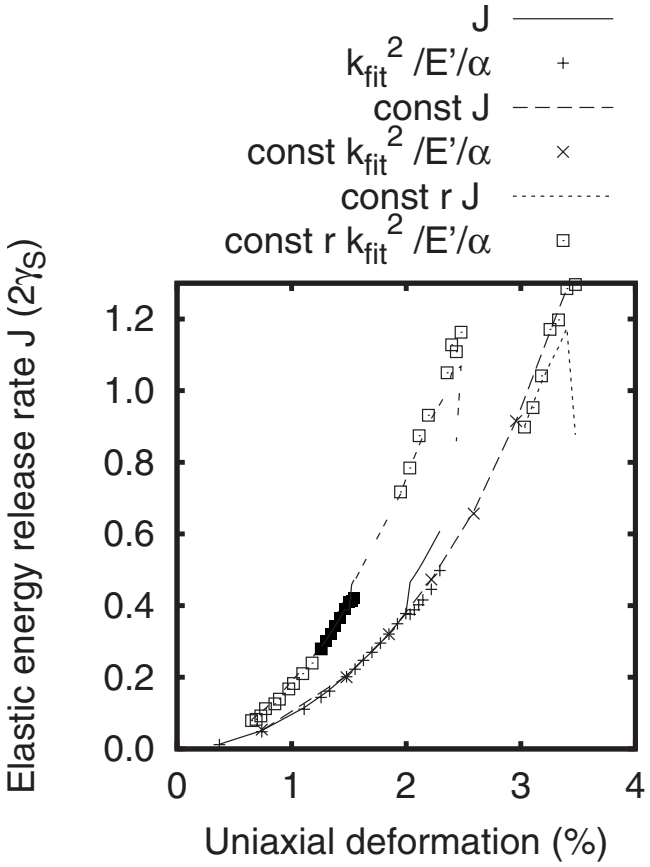

FIG. 4. Evolution of the elastic energy release rate (G) as a function of the deformation of the box for two system sizes (left curve, big box; right curve, small box). G is measured by the J integral and by k_{fit}^2/E', where k_{fit} is a measure of the stress intensity factor, obtained by a fit of the virial stress profile to the Inglis analytical solution. The legend refers only to the simulations done on the small box, right curve (similar results are obtained on the big box, left curve). The simulations under constraint are labeled "const," whereas those under constraint and with fully restored interactions (no bonds cut along the crack) are labeled "const r." Constrained cracks propagate when $G > 2\gamma_S$. The constant α is determined numerically to obtain a good match between k_{fit} and J (see text).

$=0$ K and when the strain gradients are not too large (typically, not in the core of grain boundaries), it corresponds to the Cauchy stress of the continuum.[32,33] For the specific geometry of our system, it is possible to fit the Inglis solution to the virial stress profile σ_{zz} along y in the crack plane. The crack length ($2\tilde{a}$) and the stress at infinity (σ_{zz}^{∞}) are fitted since the displacement, and not the stress, is imposed. Then, the stress intensity factor is defined as $k=\sigma_{zz}^{\infty}\sqrt{\tilde{a}/2}$. The drawback of this method is that the critical k for crack propagation ($k_{I,c}$) is only known for a limited number of situations where elastic solutions are available and make the link between k and the elastic energy release rate (G). For example, for a flaw in an infinite isotropic medium, in plane strain, $G=\frac{k_{I,c}^2}{E'}=2\gamma_s$ if the crack follows the Griffith criterion. A more systematic characterization of the applied load can be obtained by computing the J integral introduced by Rice:[34]

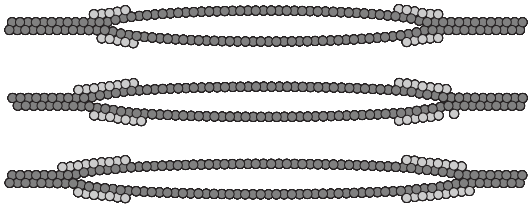

FIG. 5. Crack propagation just above $k_{I,c}$. The threshold on the CS parameter is $0.05a_0^2$. The particles of the {111} planes immediately above and below the crack plane are represented in dark gray. The light gray circles represent the constrained particles. Note that the region where the constraints operate follows the crack tip movement.

$$J=\int_{\Gamma}\left[wdx_2-\vec{T}\cdot\frac{\partial\vec{u}}{\partial x_1}ds\right], \tag{11}$$

where w is the elastic energy density and Γ is a closed path containing the crack tip [Fig. 1(b) shows the square path used in this work]. The starting and ending points of Γ are located on the fracture surface where the excess energy is due not only to elastic distortions but also and mainly to the lower coordination of the particles. Therefore, in order to consider only the elastic energy, the excess energy of the particles staying at a distance closer than $\sqrt{3}a_0$ from the surface is set to zero for the calculation of J. The tractions $\vec{T}$ are computed from the virial stress tensor. The J integrals obtained this way are not strictly path independent but converge as the circuits become wide enough. For comparison between the two methods of measuring the mechanical load, k_{fit}^2/E' and J are plotted as a function of the uniaxial deformation of the box $\bar{U}/L_0$ (Fig. 4), where $\bar{U}$ is the imposed displacement at the boundary and L_0 is the length of the box in the z direction.

The agreement between the two calculations is excellent provided k^2/E' is divided by a factor $\alpha=1.35$ (Fig. 4). α is constant for the two box sizes that we have tested. The relation $J=k^2/E'$ is universal, since it is obtained by integration of the elastic fields in the vicinity of the crack tip, where the asymptotic solution is valid. One possible explanation for this α factor is that the potential is not exactly isotropic. The variation of G according to the deformation is parabolic until the first partial dislocation is emitted, at $J\approx 0.4\times 2\gamma_S$. In Fig. 4, emission occurs when the lines diverge from the crosses, that is, when the measures of elastic energy release rate J and the local k (k_{fit}) are not coherent anymore. The divergence is also triggered by the propagation of the constrained crack; the static J is then no longer a valid measure of the energy dissipation since the solid is not in static mechanical equilibrium. Big crosses and squares on the right curve of Fig. 4 refer to constrained cracks with and without screening of the interactions between the particles along the original crack. It is recalled here that a sharp crack is an unstable object which heals if loaded below the critical load. Therefore, a sharp crack can be studied with fully restored interactions only in the vicinity of $k_{I,c}$.

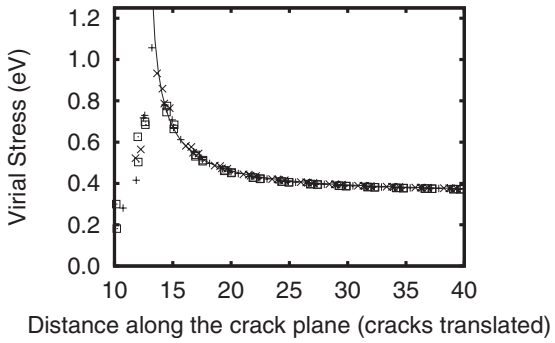

FIG. 6. Superposition of the virial stress profiles of the three cracks of Fig. 5 (the crack is translated by the position of the crack tip obtained by a fit to the elastic solution for a static crack). The fit to the Inglis solution is also presented (solid line). Multiply by 9.8 to have GPa.

We now detail the behavior of constrained cracks. The next nearest neighbors of the crack plane are scanned at every time step. As soon as the order parameter crosses the threshold, the particle i is constrained such that CS_i cannot increase any further. In order to constrain the minimum number of degrees of freedom, only the neighbors participating to the definition of the local shear (that is, the pairs which are not parallel to the glide plane of the dislocation) are considered. As seen in the constrained curve of Fig. 3, the load can be increased much beyond $k_{I,e}$ until the crack starts to propagate.

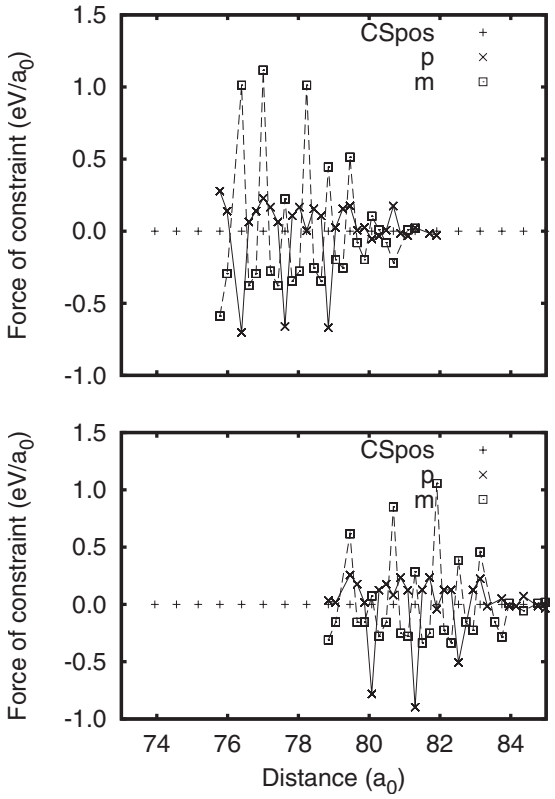

FIG. 7. Profile of forces of constraints during brittle crack propagation (to the right). (+) Position of the particles along the y axis (parallel to the crack plane); (×) force profile of the upper plane; (□) for profile of the lower plane. The oscillation of the profiles shows how the constraints create shear forces, widely distributed over the particles, to counterbalance the strong tendency to localize the shear at the emergence of the partial dislocation.

In Fig. 5, three snapshots of the brittle crack, during propagation just above $k_{I,c}$, are shown. In light gray, we represent the particles constrained with a $0.05a_0^2$ threshold. As the constrained particles are determined at each integration time step (after the positions have been updated by the Verlet algorithm), the particles are constrained in a moving window following the crack tip during propagation. As can be seen in Fig. 6, the virial stress profile of the propagating crack is remarkably stable. Figure 7 shows the constraint force "time" evolution. The constrained particles are identified by their position in the y direction, represented by crosses on the horizontal axis. However, their neighbors also feel forces of constraints [Eq. (5)], so the force profile includes both type of particles. The main feature is that the maximum amplitude is found on the constrained particles and that the profile oscillates; that is, a constrained particle is subjected to a strong configurational force, while its neighbors experiment forces of the opposite sign, with a lower amplitude (the force is distributed between the neighbors). It is very intuitive to see that this force distribution creates local shears which counterbalance the tendency of the crystal to emit dislocations. The amplitude goes to zero in front of the crack but not at the back of it. This is a consequence of the moving window which frees abruptly the particles when they are too far from the tip of the crack. In the case of static cracks, the damping of the amplitude is seen on both sides of the profile.

The value of the critical load for crack propagation lies between 1.50 and 1.59 eV/a_0^2 which remarkably encloses the surface energy $2\gamma_S = 1.55\ \mathrm{eV}/a_0^2$. The Griffith criterion is therefore valid. It is so because the forces of constraint do not influence the energy balance. This comes from a general property of holonomic constraints (constraints that depend only on particle positions) which do not produce any work.[20,21]

In this section, we have shown that the centrosymmetry parameter CS_i can be used to measure accurately the critical load to emit a dislocation from the tip $k_{I,e}$. This parameter can also be used as a constraint in MD to study cleavage and measure $k_{I,c}$. Without any surprise (Al is ductile), the crack configuration considered here is intrinsically ductile ($k_{I,e} < k_{I,c}$). Furthermore, the connection between atomistics and elasticity is made: the mechanical load at the crack tip is characterized by the stress intensity factor measured by fitting the Inglis solution on the virial stress profile and by the direct calculation of the Rice integral J. The relation between k_{fit} and J is established numerically and the overall coherence is checked when brittle propagation is obtained for $J = 2\gamma_S$, in agreement with the Griffith criterion, which should be valid for sharp cracks. Finally, we stress that only static or quasistatic cracks, loaded step by step, are studied. Dynamic cracks can be qualitatively different: brittle propagation at low velocities can become ductile when the strain energy (potential and kinetic) builds up at higher velocities around the tip.[35] The temperature dependence of dynamic dislocation emission has been probed by adding a viscous damping term to the equations of motion. This method was efficient to

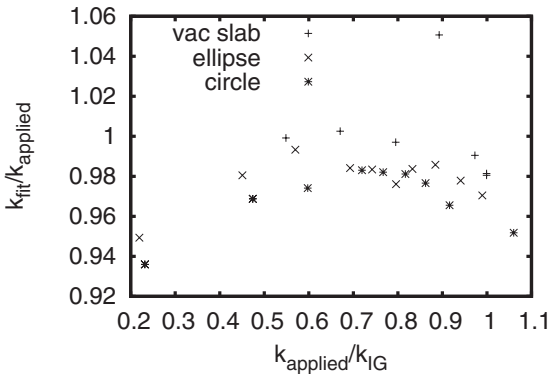

FIG. 8. Comparison of the stress intensity factor k_{fit} with the applied stress intensity factor k_{app} for different shapes of the tip: (+) a vacancy slab ($a=8a_0$), (×) an elliptical hole ($a=8a_0$, $b=4a_0$), and (*) a circular hole ($a=8a_0$).

prove that the process was thermally activated. It is an interesting complement to the approach we have developed here which is based on force control rather than kinetic energy control.

IV. BLUNTED CRACKS

We now turn to an important aspect of semibrittle fracture: crack propagation from a blunted crack tip. Beltz *et al.*[36] proposed that blunting can influence the crossover between intrinsic ductility and brittleness and therefore that a criterion for classifying materials should consider the steady shape of the tip. The shape effect on the stress profile is investigated in Ref. 37. Conclusion drawn from this work is that continuum theories describe well the stress profile (including the effect of the tip radius), except in the vicinity of the crack tip (the maximum stress concentration). Following these results, we will characterize the response of the blunted tip by k_{fit}, obtained by fitting the stress profile, notably ahead of the tip, where it follows the Inglis solution. The maximum stress will not be considered. Studies of crack reinitiation, in brittle orientations of the fcc crystal, have shown only a modest influence of the crack shape.[37,38] The maximum increase of the critical load is of the order of 30% of $k_{I,c}$ of the sharp crack. Finally, a blunted crack which retains a sharp corner preserves the stress concentration of a sharp crack, although in some cases, the stress field is distorted in such a way that dislocation emission is favored.[39] This point meets the model proposed in Ref. 36.

Blunting can be obtained by emitting a dislocation from the tip itself or by dislocations gliding in planes which intersect the tip. In the present geometry, it is possible to emit a perfect dislocation, at $T=0$, by superimposing a small mode III to a preexisting load in mode I, slightly above $k_{I,e}$. In this case, the new crack tip geometry is the same as if a slab of particles was removed. Of course, the load is complex, since the elastic field includes the external mode I and III loads and the shielding from the dislocation. We can study the response of such crack tip by creating it artificially by inserting a slab of vacancies perpendicular to the ⟨111⟩ traction axis. To have a more general view of the effect of crack

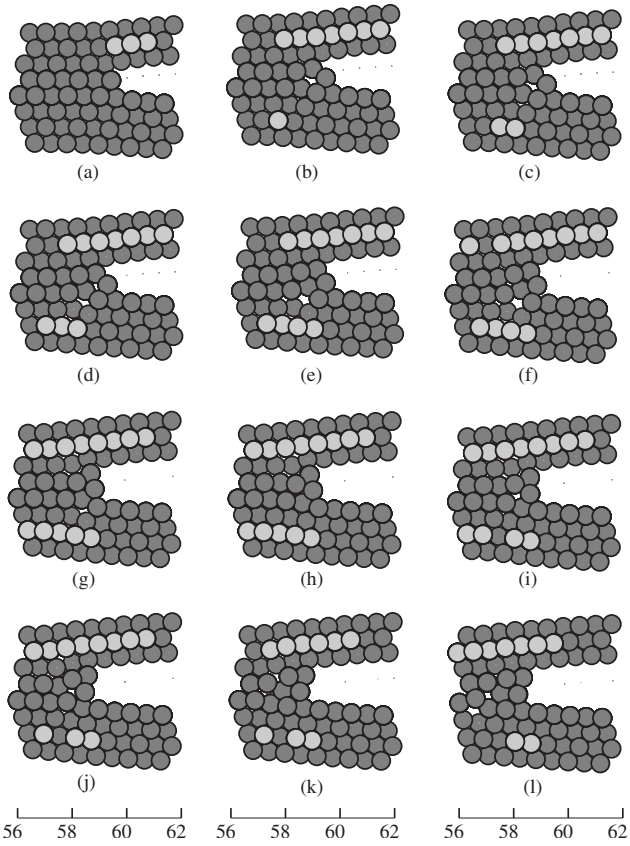

FIG. 9. Crack propagation to the left by vacancy injection mechanism (climb). The stress profiles and stress maps are given in Figs. 10 and 11. (f) one vacancy injected; (l) two vacancies injected.

blunting, we also study the response of an elliptical hole of dimensions $a=8a_0$ and $b=4a_0$, the long axis $2a$ being perpendicular to the traction axis, as well as a circular hole of radius $a=8a_0$. The constraint is turned on and the load is increased until the theoretical elastic limit is reached (a dislocation dipole is spontaneously emitted,[40] in the bulk, away from the planes of constraint) or a crack initiates.

The response of the tip is characterized by the comparison of the J integral, which represents the applied load, and k_{fit}, which is a local measure of the stress singularity. J is measured directly and transformed into an applied stress intensity factor k_{app} by the formula for the sharp crack (Fig. 4). Therefore, k_{app} represents the stress singularity that a sharp crack would feel when submitted to the same applied load as the blunted tip. For the vacancy slab, k_{fit} and k_{app} are not significantly different (Fig. 8), in agreement with previous work.[37,38] The point which departs from the general trend indicates the onset of the tip rearrangement, which is detailed below. The elliptical and circular holes also show very small differences, of the order of 2% with respect to a sharp crack (of course, the stress is no longer singular and this makes a big difference).

When k_G is reached, in the case of the vacancy slab, two different behaviors are observed: the classical brittle crack reinitiation or a restructuration of the tip that we call "vacancy injection." This last mechanism is found to begin at a slightly lower load than k_G, but this value is not really sig-

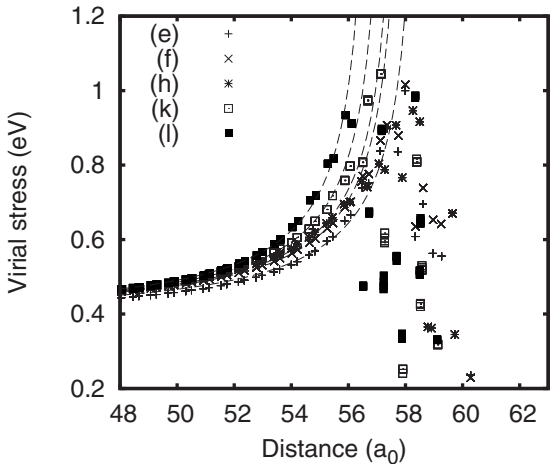

FIG. 10. Stress profiles associated with the vacancy mechanism of Fig. 9. The translation of the profile between configurations (f) (one vacancy) and (l) (two vacancies) shows the extent of the "crack propagation" induced by the vacancy injection. The lines represent the fits to the Inglis solution which show that k is constant during the process.

nificant since temperature is expected to lower the critical load for this mechanism which is "diffusionlike." A similar behavior (surface rearrangement, injection of a vacancy ahead of the tip, and then further vacancy nucleation) is observed for the elliptical and circular holes. However, in theses geometries, brittle initiation is not observed, even beyond k_G. It is remarkable that brittle propagation and vacancy injection start roughly at the same load level. It means that the vacancy mechanism is a competing mechanism, at least for the present potential.

A movie of the crack "propagating" by vacancy injection is shown in Fig. 9. From (a) to (f), the first vacancy is created when the crack tip rearranges. The premise of a new atomic layer is created. This extra layer releases the stress at the crack tip, as shown on the profiles in Fig. 10. In the frames (g)–(l), the tip further rearranges in order to create a second vacancy. The extra layer now contains two atoms. The stress singularity is stable ($0.98k_G$) and translates in front of the zone where the vacancies are located (a distance scale makes the link between Figs. 9 and 10). The two extra atoms are packed in an fcc structure. Whether the crack propagates or not is a question of semantics, since the crack tip is visibly rounded (it blunts), but the stress singularity is preserved and moves ahead of the tip. An approximate energy balance can be made easily: The creation of the first vacancy is related to the tip rearrangement which brings one atom at the surface of the tip, creating a {111} facet of surface $\sqrt{2}/2\sqrt{3/2}a_0^2$. The energy cost is therefore $\sqrt{2}/2\sqrt{3/2}\gamma_S a_0^2 + E_f^v$. The stress maps in Fig. 11 and the fit of the stress singularity in Fig. 10 show that the stress field is translated (it remains self-similar), so the elastic energy released is simply G multiplied by the crack advance. We identify an elementary crack advance to the length of the zone which is affected by the creation of a new vacancy. A rough estimate can be obtained by comparing frames (a) and (h). The tip atom moves by $\sqrt{6}/6a_0$. Furthermore, the vacancy is created and stabilized two atomic rows ahead of the tip. We can make an analogy with a Frenkel pair where the displaced atom is not in first neighbor position of the vacancy, but one neighbor shell further away. The order of magnitude of the crack advance due to the pair "displaced atom-vacancy" is therefore $3\sqrt{6}/6a_0$, which is consistent with the profile translation between (h) and (l) (related to the formation of the second vacancy) in Fig. 10. Finally, the energy balance can be written as

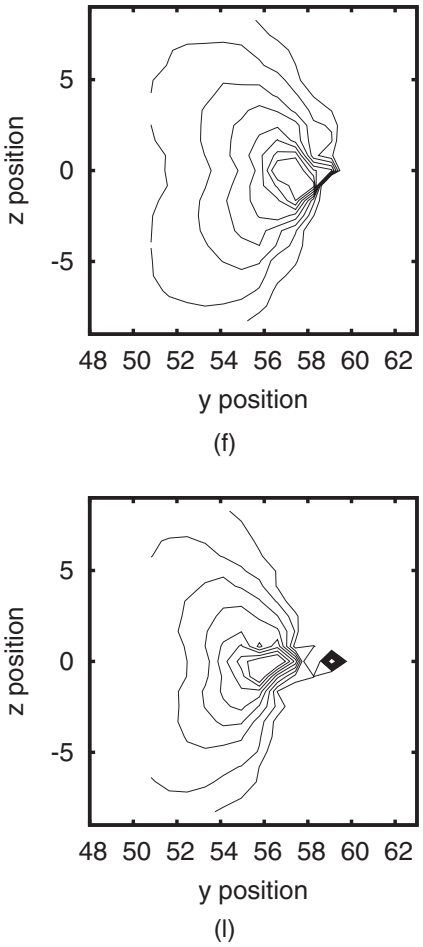

FIG. 11. Stress maps associated with the vacancy nucleation mechanism of Fig. 9, frames (f) and (l). The stress field remains roughly self-similar during vacancy injection. The isostress contours range from 0.45 eV (4.5 GPa) to 0.8 eV (8 GPa) with regularly spaced steps of 0.05 eV (500 MPa).

$$\gamma_S \frac{\sqrt{2}}{2}\sqrt{\frac{3}{2}}a_0^2 + E_f^v = G \times 3\frac{\sqrt{6}}{6}\frac{\sqrt{2}}{2}a_0^2. \tag{12}$$

This equation shows, qualitatively, that vacancy injection starts at $G=2\gamma_S$ when $E_f^v \approx \gamma_S a_0^2$, which is the case for our Al model ($E_f^v=0.7$ eV and $\gamma_S a_0^2=0.77$ eV). Equation (12) gives a simple criterion to check if this mechanism can be activated. It works in Ni, for example ($E_f^v=1.6$ eV and $\gamma_S a_0^2 \approx 1.5$ eV). According to this mechanism, chemical impurities which lower the formation energy of the vacancy could have a drastic effect (we can think of hydrogen and superabundant vacancies). However, Eq. (12) does not say anything about the energy barriers that have to be overcome. It has the same drawbacks as the Griffith energy balance. The

last point is that once the first atom of the new layer is placed at the tip, the first term in Eq. (12) drops and the energy balance is strongly in favor of the nucleation of vacancies, which means that after the first vacancy is injected, the crack can "propagate" at a lower load.

What happens to the vacancies ahead of the tip? They cluster and the ligament in between them and the main crack breaks. This kind of process has been observed previously in static[41] and dynamic[42] cracks along grain boundaries (GBs). These GBs are composed of a mixture of structural units arranged in a periodic way, some of them less cohesive than the others. They fail and generate holes which coalesce with the main crack. They also exist in brittle single crystals when the dynamic crack reaches a high velocity and starts "zigzagging."[43] Recent large scale simulations have shown that this behavior critically depends on the nonlinearity of the stress-strain relation when the size of the "nonlinear zone" is of the same order as the size of the zone where the energy is released dynamically.[44] We show here that this kind of mechanism is an alternative to pure cleavage in static (slow) transgranular cracks. It has to be stressed again that it has been obtained by frustrating the plastic behavior, which remains the natural dissipation mechanism. How these two interplay during semibrittle crack propagation has to be modeled at a higher scale, using a model for the formation of the plastic zone. It would give the amount of local deformation needed to harden the crystal ahead of the tip so that dislocation shielding is no longer enough to prevent the local k_I to reach $k_{I,c}$.[4,5]

V. CONCLUSION

We have developed a method for quantifying the proximity of a transition from intrinsic ductility to brittleness. An order parameter is used to characterize the shear localization at the crack tip. It is used as a holonomic constraint in molecular dynamics simulations. The grace of holonomic constrains is that they generate configurational forces which do not produce any work. It is particularly interesting in the context of crack propagation since it guarantees that the critical elastic energy release rate is not directly influenced by the forces of constraint. The method is applied to brittle crack initiation from blunted tips. Although we have not found a significant influence of the shape of the tip on the stress profile, it does have an important effect on the mechanism of crack advance: crack tip rearrangements are favored when the tip is blunted. The crack can propagate, at least in the case of a vacancy slab, in a brittle way by the combined nucleation of vacancies ahead of the crack tip, the formation of an extra layer of particles, and finally, the brittle fracture of the ligament between the vacancy affected zone and the "tip." This mechanism, called "vacancy injection," happens to start at a load level close to $k_{I,G}$, which means that it is a valuable alternative to cleavage. However, these results are obtained at $T=0$ and in a 2D configuration, which implies that a whole line of vacancies is injected with obvious consequences on the elastic energy released. Further work, at higher temperature, is therefore needed to confirm such mechanism.

ACKNOWLEDGMENTS

It is a pleasure to thank Ramon Ravelo, Brad Holian, Michel Mareschal, Frédéric Barmes, and Bernard Legrand who have made a lot of friendly and useful comments on this work. This work is supported by the French National Agency (ANR-06-BLAN60231).

*tanguy@emse.fr

[1] S. G. Roberts, in *Multiscale Phenomena in Plasticity*, edited by J. Lépinoux, D. Mazière, V. Pontikis, and G. Saada (Kluwer Academic, Dordrecht, 2000), p. 349.
[2] N. J. H. Holroyd, in *EICM Proceedings*, edited by R. P. Gangloff and M. B. Ives (NACE, Houston, TX, 1990), p. 311.
[3] D. Lassila and H. K. Birnbaum, Acta Metall. **35**, 1815 (1987).
[4] I. H. Lin and R. Thomson, Acta Metall. **34**, 187 (1986).
[5] V. S. Deshpande, A. Needleman, and E. V. der Giessen, Acta Mater. **51**, 1 (2003).
[6] J. R. Rice and R. Thomson, Philos. Mag. **29**, 73 (1974).
[7] A. George and G. Michot, Mater. Sci. Eng., A **164**, 118 (1993).
[8] J. R. Rice, J. Mech. Phys. Solids **40**, 239 (1992).
[9] R. Thomson and A. Carlsson, Philos. Mag. A **70**, 893 (1994).
[10] S. J. Zhou, A. E. Carlsson, and R. Thomson, Phys. Rev. Lett. **72**, 852 (1994).
[11] R. Thomson, Phys. Rev. B **52**, 7124 (1995).
[12] R. Pérez and P. Gumbsch, Phys. Rev. Lett. **84**, 5347 (2000).
[13] M. Ludwig and P. Gumbsch, Acta Mater. **46**, 3135 (1998).
[14] C. L. Kelchner, S. J. Plimpton, and J. C. Hamilton, Phys. Rev. B **58**, 11085 (1998).
[15] S. J. Zhou, A. E. Carlsson, and R. Thomson, Phys. Rev. B **47**, 7710 (1993).
[16] J. P. Ryckaert, G. Ciccotti, and H. J. C. Berendsen, J. Comput. Phys. **23**, 327 (1977).
[17] G. Ciccotti, M. Ferrario, and J. P. Ryckaert, Mol. Phys. **47**, 1253 (1982).
[18] J. P. Ryckaert and G. Ciccotti, J. Chem. Phys. **78**, 7368 (1983).
[19] S. Melchionna and G. Ciccotti, J. Chem. Phys. **106**, 195 (1996).
[20] G. Ciccotti and M. Ferrario, J. Mol. Liq. **89**, 1 (2000).
[21] H. Goldstein, *Classical Mechanics*, 2nd ed. (Addison-Wesley, Reading, MA, 1980).
[22] F. Cleri, S. R. Phillpot, D. Wolf, and S. Yip, J. Am. Ceram. Soc. **81**, 501 (1998).
[23] A. Aslanides and V. Pontikis, Philos. Mag. Lett. **78**, 377 (1998).
[24] G. Lu, D. Orlikowski, I. Park, O. Politano, and E. Kaxiras, Phys. Rev. B **65**, 064102 (2002).
[25] R. L. Hayes, M. Ortiz, and E. A. Carter, Phys. Rev. B **69**, 172104 (2004).
[26] E. A. A. Jarvis, R. L. Hayes, and E. A. Carter, ChemPhysChem **1**, 55 (2001).
[27] D. E. Jiang and E. A. Carter, Acta Mater. **52**, 4801 (2004).
[28] W. R. Tyson and W. A. Miller, Surf. Sci. **62**, 267 (1977).
[29] D. Tanguy and N. Chanon (unpublished).

[30] F. Cleri, S. Yip, D. Wolf, and S. R. Phillpot, Phys. Rev. Lett. **79**, 1309 (1997).
[31] A. Mattoni, L. Colombo, and F. Cleri, Phys. Rev. B **70**, 094108 (2004).
[32] M. Zhou, Proc. R. Soc. London, Ser. A **459**, 2347 (2003).
[33] S. Kohlhoff, P. Gumbsch, and H. F. Fischmeister, Philos. Mag. A **64**, 851 (1991).
[34] J. R. Rice, in *Fracture*, edited by H. Liebowitz (Academic, New York, 1968), Vol. 2.
[35] B. L. Holian and R. Ravelo, Phys. Rev. B **51**, 11275 (1995).
[36] G. E. Beltz, D. M. Lipkin, and L. L. Fischer, Phys. Rev. Lett. **82**, 4468 (1999).
[37] A. Paskin, B. Massoumzadeh, K. Shukla, K. Sieradzki, and G. J. Dienes, Acta Metall. **33**, 1987 (1985).
[38] P. Gumbsch, J. Mater. Res. **10**, 2897 (1995).
[39] J. Schiøtz, L. M. Canel, and A. E. Carlsson, Phys. Rev. B **55**, 6211 (1997).
[40] M. de Koning, W. Cai, and V. V. Bulatov, Phys. Rev. Lett. **91**, 025503 (2003).
[41] D. Farkas, Philos. Mag. A **80**, 1425 (2000).
[42] V. Yamakov, E. Saether, D. R. Phillips, and E. H. Glaessgen, Phys. Rev. Lett. **95**, 015502 (2005).
[43] F. F. Abraham, D. Brodbeck, R. A. Rafey, and W. E. Rudge, Phys. Rev. Lett. **73**, 272 (1994).
[44] M. J. Buehler, F. F. Abraham, and H. Gao, Nature (London) **426**, 141 (2003).